Harmonic patterns embedding ictal EEG signals in focal epilepsy: new insight into the epileptogenic zone

Lingli Hu,[1,2] Lingqi Ye,[1] Hongyi Ye,[1] Xiaochen Liu,[3] Kai Xiong,[4] Yuanming Zhang,[3] Zhe Zheng,[5] Hongjie Jiang,[5] Cong Chen,[1] Zhongjin Wang,[1] Jiping Zhou,[6] Yingcai Wu,[4] Kejie Huang,[3] Junming Zhu,[2,5] Zhong Chen,[7] Meiping Ding,[1] Dongping Yang,[8*] Shuang Wang[1,2*]

Author affiliations:

1 Department of Neurology and Epilepsy Center, Second Affiliated Hospital, School of Medicine, Zhejiang University, Hangzhou, China

2 Nanhu Brain-computer Interface Institute, Hangzhou, China

3 College of Information Science and Electronic Engineering, Zhejiang University, Hangzhou, China

4 School of Computer Science and Technology, Zhejiang University, Hangzhou, China

5 Department of Neurosurgery, Second Affiliated Hospital, School of Medicine, Zhejiang University, Hangzhou, China

6 Department of Neurology, Wayne State University/Detroit Medical Center, Detroit, MI, USA

7 Key Laboratory of Neuropharmacology and Translational Medicine of Zhejiang Province, School of Pharmaceutical Sciences, Zhejiang Chinese Medical University, Hangzhou, China

8 Research Center for Frontier Fundamental Studies, Zhejiang Lab, Hangzhou, China

***Correspondence to** :

Shuang Wang*

Department of Neurology and Epilepsy Center, Second Affiliated Hospital, School of Medicine, Zhejiang University, Hangzhou 310009, China.

E-mail: wangs77@zju.edu.cn.

Dongping Yang*

Research Center for Frontier Fundamental Studies, Zhejiang Lab, Hangzhou 311100, China.

E-mail: dpyang@zhejianglab.com.

Keywords: harmonic pattern; ictal EEG; epileptogenic zone; nonlinear phenomena; epilepsy surgery.

Abstract

The EEG biomarkers for identifying epileptogenic zone (EZ) need further refinement. Through time-frequency analysis, we identified a unique ictal spectral structure, referred to as the “harmonic pattern” (H pattern), during seizure onset or propagation in stereo-EEG signals of focal epilepsy patients. The H pattern, observed within specific EEG segments, often appeared simultaneously across different brain regions at a consistent fundamental frequency, highlighting a crucial stage in seizure propagation characterized by inter-regional synchronization. The dominant H pattern, which is identified as those above the third quartile of band numbers, demonstrated greater nonlinearity compared to the non-dominant H pattern, as evidenced by bispectral analysis. The waveforms associated with the dominant H pattern were more stereotyped and showed increased skewness and/or asymmetry. Remarkably, the complete removal of areas exhibiting the dominant H pattern was independently associated with favorable surgical outcomes. The H pattern provides unique insights into ictal neural dynamics and introduces a novel approach for measuring the EZ over an extended time window.

Impact statement

Hu et al. report that this distinct nonlinear spectral feature signifies a stereotyped waveform change and identifies a 'uniform frequency component' within the ictal network as a key stage of seizure propagation.

Introduction

Epilepsy is a chronic brain disorder characterized by paroxysmal episodes of behavioral, psychiatric, or neurological symptoms, resulting from abnormal, excessive, and synchronous cortical neuronal activity, as observed on electroencephalography (EEG). The epileptogenic zone (EZ), defined as the primary site of ictal discharge organization, refers to the areas of excessive synchronization at seizure onset (Bancaud et al., 1970). Complete removal of this zone is crucial for achieving favorable surgical outcomes in cases of drug-resistant focal epilepsy (Jehi, 2018). Intracranial EEG (iEEG) offers the highest accuracy for localizing EZ (Jin, So, & Wang, 2016). However, the ictal patterns observed on iEEG exhibit significant heterogeneity in terms of onset morphology, evolution, and propagation, suggesting a complex, highly dynamic, and individualized nature of the ictal network (Devinsky et al., 2018). The interpretation of these patterns primarily relies on visual inspection. Among individuals who undergo iEEG evaluation followed by resective or other destructive surgery, approximately 50-70% achieves prolonged seizure freedom (He et al., 2022; Sivaraju et al., 2022), which is still considered unsatisfactory.

Several quantitative EEG methods have been developed to improve the delineation of EZ, complementing the traditional visual inspection of ictal iEEG (Frauscher, 2020). Most of these studies utilize fast activity (FA, usually > 30 Hz), on its own or combined with other features (Bartolomei, Chauvel, & Wendling, 2008; David et al., 2011; Gnatkovsky et al., 2014; Gnatkovsky et al., 2011; Hu et al., 2023; Wetjen et al., 2009; Wilke, Worrell, & He, 2011). For example, the epileptogenic index or epileptogenicity mapping, which assesses alterations in the energy ratio between fast and slow activity

on stereo-EEG (SEEG) signals occurring at the early onset of a seizure, provides a quantitative measurement for identifying EZ (Bartolomei et al., 2008; David et al., 2011). On the other hand, recent studies showed that the spectral structure of the ictal FA is as important as its power (Di Giacomo et al., 2024; Grinenko et al., 2018). For example, the term “ictal chirp” refers to a narrow band of high-power FA (> 80 Hz) on a time-frequency map (TFM) with decremental frequency over 5-10 s. This pattern is common and might help localize EZ in focal epilepsy (Di Giacomo et al., 2024; Schiff et al., 2000). Grinenko et al. proposed the concept of EEG fingerprints as ictal markers for identifying the EZ (Grinenko et al., 2018; Li et al., 2020). They discovered that ictal FA comprises multiple narrow bands rather than broad-band activity. However, these methods are less effective for slower EEG seizure onset patterns (SOP), which account for 20-30% of the common onset patterns observed on iEEG (Balatskaya et al., 2020; Lagarde et al., 2019; Singh, Sandy, & Wiebe, 2015). The spectral properties of ictal EEG, relevant to various SOPs, need further investigation to improve the accuracy of EZ localization.

In this study, we conducted a comprehensive analysis of the spectral properties of ictal iEEG in focal epilepsy, aiming to uncover potentially useful characteristics for EZ localization. We identified a unique and common spectral structure, referred to as the “harmonic pattern” (H pattern), which is characterized by multiple equidistant, high-density bands with varying frequencies over time (Fig. 1). The H pattern is commonly observed in ictal EEG recordings from both experimental models of epilepsy as well as epileptic patients (Lévesque, Herrington, Hamidi, & Avoli, 2016; Lévesque, Salami, Gotman, & Avoli, 2012; Schiff et al., 2000). However, it has not been systematically studied. Notably, the presence of harmonics as a spectral feature of EEG or local field potential (LFP) often indicates that

neural oscillations are nonsinusoidal and possibly carry overlooked, nonlinear components that are indicative of neural communication patterns (S. R. Cole & Voytek, 2017). Importantly, the nonlinear nature of the brain has long been recognized as fundamental to large-scale integration among local neurons, facilitating rapid neuronal organization that supports behavior (Sheremet, Burke, & Maurer, 2016). Understanding and quantifying brain nonlinearity is essential for translating brain dynamics into behavior (Buzsa´ki, 2006; Sheremet et al., 2016). Therefore, it is necessary to further investigate whether harmonics can reveal the nonlinear nature of the ictal network.

To better clarify the clinical relevance of the H pattern, we examined the characteristics of the initial H pattern and its clinical significance in a cohort of individuals with focal epilepsy who underwent iEEG evaluation. Our findings indicate that the H pattern encapsulates clinical relevance for EZ localization as well as seizure propagation. Moreover, we delved into the signal properties of the H pattern to uncover its potential generation mechanisms using bispectral analysis, a type of higher-order spectral analysis.

Results

Patients and iEEG evaluation

We analyzed iEEG data from all patients who underwent iEEG evaluation between January 2014 and April 2021 (n = 80). Three patients were excluded due to insufficient clinical and ictal EEG information, and another seven were excluded because their seizure onset origins could not be localized. In the end, data from 70 patients were available. To investigate the association between the H pattern and seizure onset patterns (SOP), the SOPs of all seizures were classified into six types (Fig. 1*A*):

Pattern 1, 36 cases with preictal spikes/sharps/polyspikes following fast activity > 14 Hz;

(a) Pattern 1.1: low-voltage fast activity (LVFA), amplitude < 30 μV;

(b) Pattern 1.2: high-voltage fast activity (HVFA), amplitude ≥ 30 μV.

Pattern 2, 11 cases with slow wave/DC shift followed by LVFA;

Pattern 3, 12 cases with spikes activity;

Pattern 4, seven cases with LVFA;

Pattern 5, three cases with beta activity;

Pattern 6, one case with delta-brush.

After a follow-up period of 35.5 ± 21.3 months, 48 patients (68.6%) achieved seizure freedom.

We reviewed TFM during the ictal periods for the 70 patients. Of these, 57 patients presented with at least one H pattern, while the remaining 13 patients did not show any discernable H pattern. Importantly, the routine visual inspection was unable to differentiate the EEG segments harboring the H patterns from those without, in the absence of TFM. The H pattern could occur at different stages of the ictal phase, and their ictal SOPs could be all patterns except delta-brush (Fig. 1*A*-*C*). No difference was found between the H pattern and non-H pattern groups in terms of SOP (P = 0.095, Fisher exact test), lobar origin (P = 0.475, Fisher exact test), presence of MRI lesion (85.9 % vs. 76.9 %, P = 0.416, Fisher exact test) or seizure freedom (68.4 % vs. 69.2 %, P = 1.000, Fisher exact test). The most common pathological finding in both groups was focal cortical dysplasia II (FCD II) (49.1 % vs. 38.5 %, Fisher

exact test). In the end, 57 patients (81.4%) were included in the subsequent analysis of the H pattern (Fig. S1). The EZ fingerprint, as defined by Grinenko et al's methods, was observed in 25 out of the 70 patients (35.7%).

Among the 57 patients who exhibited H pattern (Table 1), there were 31 males and 26 females. The mean age of epilepsy onset was 10.4 ± 8.5 years, while the mean age at the time of surgery was 23.6 ± 12.3 years. There were 49 patients (85.9 %) who had identified lesions on MRI. The most frequent seizure origins were the frontal and temporal lobes, with FCD II being the most prevalent pathological finding (49.1%). At the final follow-up, 39 patients (68.4%) achieved seizure freedom. No differences in various features were observed between the seizure-free (SF) and not seizure-free (NSF) groups, except for pathological findings, in which significant differences were noted between FCD II and gliosis/nonspecific findings.

Classification of H pattern

The initial H pattern emerged at 18.1 ± 20.5 s after the ictal EEG onset. The onset time was not limited to the early stage of seizure evolution but occasionally extended to the late stage of seizures (Fig. 1*C*). The H patterns were specifically embedded in two types of EEG segments: fast activity > 25 Hz and irregular polyspikes > 5 Hz. Consequently, H patterns were classified into: FA-H pattern and PS-H pattern (Fig. 2*A*). The proportions of the initial H patterns observed were similar, with 30 out of 57 patients exhibiting the FA-H pattern and 27 out of 57 showing the PS-H pattern. The FA-H pattern was found to have a lower number of bands (Z = -2.75, P = 0.006, nonparametric Mann-Whitney U test) and a higher frequency interval (Z = -4.52, P < 0.0001, nonparametric Mann-Whitney U test) compared to

the PS-H pattern. In the FA-H pattern, both the start time (time zero, EEG onset time; Z = -2.85, P = 0.004, nonparametric Mann-Whitney U test) and the end time (Z = -2.43, P = 0.015, nonparametric Mann-Whitney U test) occurred earlier than those in the PS-H pattern. Additionally, the minimal frequency (Z = -5.14, P < 0.0001, nonparametric Mann-Whitney U test) and maximal frequency (Z = -2.30, P = 0.021, nonparametric Mann-Whitney U test) were higher (Fig. 2*B*). In all H patterns, the frequencies of the band varied over time, exhibiting upwards, downwards, or were bell-shaped before eventually disappearing.

Spatial distribution of H pattern and surgical outcome

The H pattern commonly occurred in the seizure onset zone (SOZ), early propagation zone (PZ), and sometimes in other zones (OZ) at very close time points, displaying nearly the same frequency interval, even when these regions were remotely separated (Fig. 3*A*-*C*). The H pattern' end time and minimal/maximal frequencies did not vary across regions. Occasionally, the H pattern extended to the ipsilateral thalamus, appearing simultaneously with cortical regions and demonstrating the same frequency interval (Fig. S2).

The proportion of contacts displaying the H pattern in each region decreased in the order from SOZ, PZ to OZ (H *(2)* = 57.16, SOZ vs PZ, P < 0.001; SOZ vs OZ, P < 0.001; PZ vs OZ, P = 0.004, nonparametric Kruskal-Wallis tests, after Bonferroni correction). Likewise, the number of bands exhibited a similar decreasing trend in each respective zone (H *(2)* = 32.69, SOZ vs PZ, P = 0.014; SOZ vs OZ, P < 0.001; PZ vs OZ, P = 0.012, nonparametric Kruskal-Wallis tests, after Bonferroni correction, Fig. 3*C*).

The H pattern in most SOZ showed the highest number of bands (Fig. 3*C*). To pinpoint H pattern regions that may indicate epileptogenicity, we defined the dominant-H pattern (*d*H pattern) regions by using Q3 as a threshold in each patient (see Methods). In the follow-up study, we compared the resection ratios of SOZ, the H pattern, the *d*H pattern, and non-*d*H pattern channels in the SF and NSF groups. The results showed that the patients in the SF group had a significantly larger resection proportion of areas expressing the *d*H pattern compared to those in the NSF group (1.00 (0) vs. 1.00 (0.56), $Z = -3.29$, $P = 0.003$, nonparametric Mann-Whitney U test, after Bonferroni correction). In contrast, no such differences were found for the SOZ, the H pattern, *or* the non-*d*H pattern (Fig. 3*D*). On multivariate analysis, after adjusting for potential confounders of pathology, a complete resection of areas expressing the *d*H pattern was significantly associated with a higher chance of seizure freedom (Fig. 3*E*).

Nonlinear analysis of H pattern

The clinical implications of the H pattern have been established in the above findings. To further investigate the mechanism behind its generation, we analyzed the signal properties. Harmonic phenomena are typically associated with nonlinear effects, but linear effects can also contribute, as both can produce equidistant frequency intervals in the spectral domain (Fig. 4*A*). However, nonlinear effects uniquely create frequency coupling, which can be detected through bispectral analysis (Fig. 4*B*-*C*). Our bispectral analysis of patients exhibiting the H pattern revealed that it is predominantly due to nonlinear effects. Additionally, the *d*H pattern exhibited stronger nonlinear effects compared to the

non-*d*H pattern (0.32 (0.94) vs 0.12 (0.28), Z = -4.21, P < 0.0001, nonparametric Mann-Whitney) (Fig. 4*D-F*).

Nonlinearity, extending beyond spectral domain features, was evident in the time domain through waveform distortions, marked by the presence of skewness and asymmetry (Fig. 4*G-H*). Specifically, skewness refers to the asymmetry of the wave along the horizontal axis, such as sharp narrow peak (trough) and broad shallow trough (peak); while asymmetry denotes the uneven distribution along the vertical axis, such as sawtooth waves (short rise (decay) and long decay (rise)) (Fig. 4*H*). In the following sections, we will carefully investigate the waveform characteristics of the EEG signals corresponding to the H pattern through four representative cases.

Stronger skewness underlying dH pattern

We initially presented a case involving the FA-H pattern (Fig. 5). The *d*H pattern exhibited more bands compared to the non-*d*H pattern (Fig. 5*A*), which was attributed to sharper troughs in the EEG signals. This was demonstrated by fitting peaks and troughs with sinusoidal waves individually (Fig. 5*C*). In the *d*H pattern, the trough durations (T_{trough}) were consistently lower than the peak durations (T_{peak}). The consistency of T_{trough} contributed to a more stereotyped waveform, highlighting its distinctive morphological consistency (Fig. 5*C*).

The nonlinearity of harmonics was assessed through bispectral analysis (Fig. 5*B*). This analysis showed that the *d*H pattern exhibited stronger bicoherence and skewness (indicative of sharper troughs), whereas these features were less pronounced in the non-*d*H pattern. To further demonstrate the role of sharper troughs in generating the H pattern, we constructed a simple waveform with sharper

troughs, which exhibited pronounced harmonics. The corresponding bispectral analysis showed strong bicoherence and skewness, confirming that sharp troughs contribute to the generation of the H pattern (Fig. S3*A-C*, left).

Stronger asymmetry underlying dH pattern

In the second case with the FA-H pattern, the *d*H pattern was generated by asymmetric waveforms. Here, the rise durations (T_{rise}) were consistently longer than the decay durations (T_{decay}) (Fig. 5 *D, F*). Both T_{rise} and T_{decay} remained constant, resulting in a relatively stereotyped EEG waveform for the *d*H pattern. The harmonic nonlinearity was also confirmed by its bispectral characteristics, which showed stronger bicoherence and asymmetry in the *d*H pattern than the non-*d*H pattern (Fig. 5*E*). Furthermore, we designed a sloping waveform characterized by longer T_{rise} compared to T_{decay}, with its TFM exhibiting strong harmonics. The bispectral analysis has strong bicoherence and asymmetry. This observation further validated the role of asymmetric waveforms in generating the H pattern (Fig. S3*A-C*, right).

Stronger skewness and asymmetry underlying dH pattern

The waveform associated with the H pattern sometimes concurrently manifested skewness and asymmetry. One more case with an FA-H pattern was presented in Fig. S4. The case revealed that the *d*H pattern was featured by sharp troughs and asymmetry (short rise, long decay) of waveforms (Fig. S4 *A, C-D*). The distorted waveforms consistently appeared for the *d*H pattern, causing to a stereotype morphology of the EEG segment. Furthermore, the harmonic nonlinearity was corroborated by the

bispectral characteristics, where the *d*H pattern exhibited stronger bicoherence, skewness, and asymmetry compared to the non-*d*H pattern (Fig. S4*B*).

We concluded by presenting a case with the PS-H pattern (Fig. 5S). This pattern was characterized by both sharp peaks and asymmetric (short rise, long decay) waveforms (Fig. 5S *A, C-D*). The highly stereotyped waveform of the *d*H pattern was attributed to its consistently sharp peaks and asymmetric pattern. Similarly, we found that the *d*H pattern exhibited stronger bicoherence, skewness, and asymmetry compared to the non-*d*H pattern, as reviewed (Fig. S5*B*).

In summary, in our study the high-order spectral analysis revealed the existence of oscillatory interactions in the H pattern, suggesting a nonlinear effect. In the time domain, the H pattern was the spectral signature of the shape change of EEG waveforms.

Propagation analysis of H pattern

Focal seizures often originate from a localized region and subsequently propagate to other brain areas. Understanding this propagation is crucial for understanding seizure dynamics. Both *d*H and non-*d*H patterns typically share the same fundamental frequency, indicating synchronized oscillations between these regions and suggesting an underlying connection.

Nonlinear features of EEG signals can be influenced during the spatiotemporal propagation between regions. The stronger nonlinear effects observed in the *d*H pattern compared to the non-*d*H pattern may reflect the process of spatiotemporal propagation from the *d*H to the non-*d*H pattern. To test this hypothesis, we used transfer functions to evaluate the relationship between the *d*H and non-*d*H

patterns. The results revealed that the peak FitPercent was higher when estimating propagation from the *d*H pattern to the non-*d*H pattern, compared to the reverse direction (42.44 (34.44) vs 22.68 (28.72), Z = -6.35, $P < 0.0001$, Wilcoxon signed-rank) (Fig. 6). This suggests that the *d*H pattern is more likely to propagate to the non-*d*H pattern, while propagation in the opposite direction occurs less frequently.

Discussion

As a distinct spectral feature of ictal iEEG signals, the H pattern was commonly observed in most patients with various EEG onset patterns, whether during early or late seizure propagation (Weiss et al., 2013). Moreover, despite substantial variations in the morphology and features of the H pattern across individuals, each patient exhibited a highly uniform pattern for habitual seizures. Its analysis not only provides crucial insights into the dynamics of ictal neural activity but also offers valuable information about the EZ. Our important findings include: (1) The dominance of H pattern is a promising and universal ictal marker for identifying the EZ; (2) the H patterns are, in fact, the spectral signature of waveform skewness or/and asymmetry, with the dominance of H pattern reflecting a stronger nonlinearity of ictal oscillations, which correlates with higher epileptogenicity (Fig.7); (3) the H patterns can occur simultaneously in different cortical regions with consistent fundamental frequencies, suggesting they represent a pivotal stage of inter-regional synchronization during seizure propagation.

Our findings not only enhance the understanding of the spectral features of ictal EEG but also underscore its significance in defining the EZ. Some of the FA-H patterns observed in our study resemble or may overlap with narrow band fast activity as defined in EEG fingerprint studies or *Chirp* studies (Grinenko et al., 2018; Schiff et al., 2000). Notably, the H pattern was also observed during later

stages of seizure propagation for PS-H patterns, sometimes in the seizures that did not have initial fast activity. This suggests the potential for expanding the time window for defining the EZ using ictal EEG. In our study, the sensitivity for detecting EEG fingerprints was low, while the ictal H pattern was prevalent. The FA-H pattern and PS-H pattern manifested during different stages of seizure evolution. Compelling evidence indicates that the presence of fast activity is supported by a significant activation of inhibitory interneurons, combined with a transient shutdown of excitatory cells (Fujiwara-Tsukamoto et al., 2010; Gnatkovsky, Librizzi, Trombin, & de Curtis, 2008; Köhling, Vreugdenhil, Bracci, & Jefferys, 2000; Lasztóczi, Nyitrai, Héja, & Kardos, 2009; Velazquez & Carlen, 1999; Ziburkus, Cressman, Barreto, & Schiff, 2006). Therefore, the FA-H pattern may be predominantly influenced by inhibitory interneurons. On the other hand, irregular spiking usually occurs at the later stage of seizures and is linked to a decrease in inhibitory interneuron firing and an increase in excitatory neuron interactions (de Curtis & Gnatkovsky, 2009). The PS-H pattern may be supported by a more substantial involvement of excitatory neuron firing.

Harmonic phenomena have a well-established presence in EEG or local field potential (LFP) signals, potentially linked to specific brain functional states (Coelli et al., 2019; Marceglia et al., 2006; Müller-Putz, Scherer, Brauneis, & Pfurtscheller, 2005). For instance, during nonrapid eye movement (NREM) sleep, sleep spindles exhibit harmonic phenomena, with parameters changing in accordance with sleep stages, reflecting functional alterations in the thalamocortical reverberant network (Abeysuriya, Rennie, Robinson, & Kim, 2014). Sheremet et al. studied the LFP recorded in the rat hippocampus and found harmonics of theta activity, together with the corresponding waveforms, changed with the movement speed of patients, harmonic phenomena have not received adequate

attention in the field of epilepsy (Lévesque et al., 2016; Lévesque et al., 2012; Schiff et al., 2000). Our finding unveils harmonic features harbor localizing information about the neural dynamics of seizures, enriching our knowledge of the ictal network and emphasizing the importance of considering the nonlinear nature of the ictal network.

Neural oscillations, as a prominent feature in brain recordings, are crucial for understanding both pathological conditions and physiological behaviors (S. Cole & Voytek, 2019; Samarasinghe et al., 2021). Traditionally, these oscillations are analyzed by linear methods, which may overlook the complexity of brain activity (Buzsa´ki, 2006). Spectral analysis often involves filtering signals into specific frequency bands of interest, treating EEG signals as if they were simple sine waves, and applying smoothing techniques. This approach can obscure or eliminate subtle waveform features. Increasing evidence suggests that neural oscillations are frequently non-sinusoidal and contain significant nonlinear information (Buzsa´ki, 2006; Sheremet et al., 2016). In this study, we demonstrated that the nonlinearity of ictal signals, as confirmed by high-order spectral analysis and corresponding to waveform skewness and/or asymmetry, can be quantified and measured. The nonlinearity was more pronounced in the *d*H pattern compared to the non-*d*H pattern. Some studies showed nonlinear analysis of ictal EEG using sophisticated algorithms could provide seizure localization information (Andrzejak, Schindler, & Rummel, 2012; Hu et al., 2023). However, the nonlinear feature of the H pattern can be directly visualized in both the time and spectral domains, offering significant practical application value. In addition, our findings highlight the importance of waveform analysis, which can complement linear methods of EZ localization based on EEG frequency and power.

Many studies suggest that non-sinusoidal waveforms in EEG can reflect the degree of correlated activity within neuronal populations. For example, sharp transients observed in spike-wave discharges are indicative of synchronous neuronal firing (Slaght et al., 2004). Recent research has shown that increased neuronal synchronization results in highly asymmetric waveforms, while reduced synchronization leads to more sinusoidal shapes (Garcia-Rosales, Schaworonkow, & Hechavarria, 2024). Additionally, a stronger nonlinear component in the EEG waveform often indicates greater neuronal synchronization in the cerebral cortex (Stam, 2005). Our results show that the *d*H pattern exhibits greater skewness and/or asymmetry in its waveforms compared to the non-*d*H pattern, with a more stereotyped waveform. This consistency suggests the repeated occurrence of the same oscillatory pattern. These findings imply that the H pattern may serve as an EEG signature of rhythmic and synchronized neuronal firing within local epileptic tissues (Fig. 7). The diverse waveforms observed during this stage could reflect various underlying neuronal mechanisms. Further research is imperative to elucidate the cellular and dynamic processes responsible for the diverse waveforms associated with the H pattern.

The H pattern represents a distinctive stage in seizure propagation. Our findings indicate a higher likelihood that signals in the *d*H pattern propagate to the non-*d*H pattern, aligning with the gradient of epileptogenicity across brain regions. The H pattern visually represents this unique stage of inter-regional synchronization, as evidenced by the consistent fundamental frequencies observed across regions during the occurrence of H pattern. This synchronization may be a characteristic of seizure propagation. Notably, this synchronization can also extend to distant areas, including contralateral cortical regions and even the ipsilateral thalamus.

The study has several limitations. First, simultaneous unit recording was not performed, which limits the exploration of the cellular mechanisms underlying the H pattern. Secondly, due to the heterogeneous morphology of H patterns across subjects and the current lack of automated identification, their visual recognition was inherently subjective to personal experience. Moreover, multiple H patterns sometimes occur in the same seizure, but only the first occurrence was analyzed in this study. Further investigation is warranted for cases where H patterns appear consecutively. Thirdly, using a threshold (Q3) to define the dominant H pattern may not accurately capture individual variability. Future studies could benefit from adopting a patient-specific approach to defining the dominant H pattern.

Conclusion

Our study defines a common and distinctive ictal spectral feature, termed the H pattern. Its dominance signifies specific waveforms and highlights the nonlinearity of ictal EEG signals. This feature may be associated with rhythm and synchronization of neuronal firing in local epileptic tissues. The H pattern imparts unique information about ictal neural dynamics as well as offers novel insights into localizing the EZ. Our data also provides evidence supporting an elongated time window for measuring EZ using quantitative EEG.

Methods

Patients and intracranial electroencephalography evaluation

We conducted a review of consecutive patients with drug-resistant focal epilepsy who underwent intracranial electroencephalography (iEEG) evaluation followed by resective surgery at our epilepsy

center between January 2014 and April 2021. All patients were followed for more than two years after surgery. A comprehensive assessment was undertaken, encompassing a detailed medical history, neuropsychological testing, neuroimaging examination, and scalp video-EEG recordings. This study was approved by the Medical Ethics Committee of the Second Affiliated Hospital, Zhejiang University School of Medicine (Study No. 2020-910). iEEG was performed using intracerebral multiple-contacts electrodes, with contacts that were 2 mm in length, 0.8 mm in diameter, and 1.5 mm apart. iEEG signal was recorded by EEG systems with 256 channels (Nihon Kohden) or 128 channels (Xltek, Natus, Ontario, Canada) at a sampling rate of 1000 or 2000 Hz. Pre-implantation MRI and post-implantation computed tomography (CT) were co-registered to locate each contact anatomically along each electrode trajectory.

EEG data were reviewed on bipolar montage. Only contacts within the grey matter were selected. SOP was assessed on the earliest involved electrodes. As previously described (Hu et al., 2023; M. Y. Wang et al., 2017; S. Wang et al., 2017), SOZ was defined as the area unequivocally showing the earliest change on iEEG, and PZ as the area showing a rapid spread of ictal activity within 3-5 seconds of seizure onset. Other brain regions were classified as OZ. SOP, SOZ, PZ, and OZ were independently defined by two clinical neurophysiologists. In the event of inconsistencies, discussions would be held with a third epileptologist to reach a consensus.

Surgical plans were developed by a multidisciplinary team, independent of the parameters considered in this study. After surgery, preoperative MRI and postoperative CT were integrated to identify precise borders of the resection. The electrode contacts located on resection margins or in disconnected

tissues were defined as removed contacts. Surgical outcomes were assessed at the most recent follow-up based on Engel's classification. Surgical outcomes were classified as Engel Ia (seizure-free, SF) and > Engel Ia (not seizure-free, NSF).

Quantitative EEG analysis

Identification of Harmonic patterns

For each seizure, a 110-second window of iEEG data was extracted: 10 s before and 100 s after the seizure onset, and another 110 s-epoch of iEEG data was also collected (> 2 min before the seizure onset) as a statistical baseline. Morlet wavelet transform analysis was used to generate TFM and subsequently validated using the multitaper method. Both methods used linear spacing in the frequency range of 1 to 300 Hz, with an interval of 1 Hz. The TFM of seizure was normalized by the baseline data, where the power at each frequency was divided by the corresponding baseline power (for methodological details, see Grinenko et al., 2018) (Grinenko et al., 2018).

The features of the H pattern are characterized by its frequency distribution, which is similar to a harmonic structure composed of multiple equidistant, high-density narrow bands with varying frequencies over time (Fig. 1*C*). Each frequency band (referring to the shape of the frequency distribution, rather than the range of frequencies in this study) of H pattern, ranging from low to high, were denoted as the first (f_{1st}), second (f_{2nd}), third frequency band (f_{3rd}), and so forth. At a specific time point, the consistent difference between adjacent frequency bands is defined as the frequency interval. This interval is equivalent to the fundamental frequency (*f*), which commonly denotes the frequency of the lowest frequency band. The frequencies of narrow bands fall around the multiples of the

fundamental frequency. The minimal and maximal frequencies were determined at the peaks of the first and last frequency bands, respectively. The parameters of the H pattern, including minimal/maximal frequency and start/end time, were extracted using Brainstorm software. For one patient, the H pattern was usually consistent in habitual seizures (Jouny, Adamolekun, Franaszczuk, & Bergey, 2007), and we randomly selected one seizure for analysis. In cases where several H patterns occurred consecutively within a single seizure, only the initial pattern was chosen for analysis.

To further identify channels exhibiting the dominant H pattern, a threshold of Q3 was set, represented as the upper quartile (75th percentile of data distribution) of the total number of bands:

$$Q3 = (n + 1) \times 3/4$$

where n is the highest band number in each individual. Any channel with a band number of H pattern exceeding this threshold would be designated as a “dominant-H pattern” (*d*H pattern) channel; otherwise it was labeled as a “non-dominant H pattern” (non-*d*H pattern) channel.

The correlation between removal of the region expressing SOZ, the H pattern, the *d*H pattern or non-*d*H pattern and the postoperative outcome was analyzed. Resection ratio was calculated as the number of channels with the events included within the resection over the total number of channels where the events were observed (S. Wang et al., 2017). A value of 1 indicates complete removal of the events, while a value of 0 represents complete non-removal.

Nonlinear analysis of H pattern

From a physical standpoint, harmonics can originate from either linear or nonlinear phenomena, each exhibiting its intrinsic characteristics. In a linear system, solutions can be superposed to construct new solutions, forming a linear space. Sinusoids make up the Fourier basis of this solution space, where the general solution is a superposition of sinusoids with varying amplitudes, fully defined by the amplitude distribution. The geometry of a linear system's solution space is straightforward: any point within the space spanned by the Fourier basis represents a solution, and the general solution is characterized by its amplitude projections on this basis. Thus, harmonics are statistically independent and their presence does not modify the statistics of the process.

Conversely, in nonlinear systems, solutions cannot be simply added to form new ones, rendering them more complex. Decomposing such systems on a linear basis results in a set of equations that describe the evolution of amplitudes through their mutual interactions. The solution space's geometry becomes intricate, with phase correlations influencing the solution shape, such as the development of time series asymmetries. Thus, the presence of harmonics might be accompanied by phase correlations that have significant and fundamental effects on the shape and statistics of the process. The spectral density alone lacks details about phases, their correlations, and the nonlinearity of the process. We can check the phase correlation between spectral components by bispectrum analysis, the basic formula is as follows:

$$B_{n,m} = B(f_n, f_m) = \mathrm{E}[G_n G_m G^*_{m+n}]$$

Here, f_n and f_m are two frequencies, G_n is the corresponding complex Fourier coefficient using the discrete Fourier transform (DFT), and * denotes the complex conjugate. The bispectrum $B_{n,m}$ represents the phase correlation between Fourier modes with frequencies f_n, f_m and $f_{n+m} = f_n + f_m$.

To eliminate the distortion induced by the variance distribution, the bispectrum can be normalized as follows:

$$b_{n,m} = \frac{B_{n,m}}{(\mathrm{E}[|G_n G_m|^2]\mathrm{E}[|G_{n+m}|^2])^{1/2}}.$$

The squared modulus and phase of the normalized bispectrum $b_{n,m}$ are termed bicoherence and biphase, respectively (Sheremet et al., 2016).

The bispectrum, and by extension the normalized bispectrum, displays well-established symmetries in the (f_n, f_m) plane, as illustrated in Fig. 4*B*. The first diagonal acts as a symmetry axis, making the data on either side equivalent (Rosenblatt, 1965). The red triangle highlights the nonredundant bispectral information, which is crucial for interpreting bispectral distributions. At any point (f_n, f_m), the value of the bispectrum B (f_n, f_m) represents the phase correlation between the Fourier modes with frequencies f_n, f_m and f_{n+m}. For a linear system, where Fourier coefficients are mutually independent, the bispectrum is statistically zero. In nonlinear systems, however, the bispectrum will exhibit peaks at triads that are phase correlated, reflecting the degree of two-wave coupling (Fig. 4*C*).

In the spectral domain, nonlinearity is expressed as the development of a chain of harmonics statistically phase coupled to fundamental frequency. In the time domain, it is expressed as the development of skewness and asymmetry in the waveform (Fig. 4*H*). To elaborate, a wave comprises

one or more periods, featuring peaks, troughs, rise and decay. Skewness indicates horizontal asymmetry, where the duration of peaks or troughs is not half the period. Asymmetry points to vertical asymmetry, with rise or decay times also not being half the period. The normalized bispectrum's real and imaginary parts encapsulate the "frequency distribution" of these waveform distortions. We will refer to the real and imaginary parts of the normalized bispectrum as the distributions of skewness and asymmetry, defined as follows:

$$\xi_{n,m} = \mathrm{Re}\{b_{n,m}\};\ A_{n,m} = \mathrm{Im}\{b_{n,m}\}$$

Here, Re{z} and Im{z} denote the real and imaginary parts of the complex number z, respectively. The sign of ξ and A ($\pm$) indicates the direction of the skewness or asymmetry.

Furthermore, waveform original iEEG signals were carefully analyzed. Initially, signals were detrended using the smoothing method 'loess' in MATLAB, which adjusted the wave's oscillations around a zero-valued baseline, thereby distinguishing troughs form peaks. Each trough and peak was subsequently fitted with a sinusoidal wave of a single frequency to identify the waveforms of EEG signals.

EEG signals were processed by de-meaning, linear detrending, and dividing into 50% overlapping segments of approximately 0.5-second windows (2^{10}-point windows at a sampling rate $f_s = 2000$ Hz), achieving a frequency resolution of approximately $\Delta f = 2$ Hz. The total intervals were around 7 seconds, yielding approximately 28 degrees of freedom (DOF). For the normalization $b_{n,m}$, the probability density function was approximated using the noncentral χ^2 distribution (S. G. Elgar S, 1989; Rosenblatt, 1965). A confidence level distinguishes linear from nonlinear stochastic processes. With

DOF = 28, zero-mean bicoherence, significant in this context, is $|b| < \sqrt{\frac{6}{DOF}} \approx 0.46$ for a 95% confidence level (G. R. Elgar S, 1985; S. G. Elgar S, 1989). All calculations were implemented in MATLAB, utilizing its DFT functions. Bispectral estimates were computed using code based on modified functions from the HOSA toolbox.

Inferring seizure propagation

We employed transfer functions to estimate the propagation relationship between the *d*H pattern and non-*d*H pattern. Using 'tfest' in MATLAB, we estimated all possible transfer functions with number of poles np and zeros nz ranging from 0 to 10 with the constraint $nz \leq np$ and enforced stability of the system. As discussed in **Nonlinear analysis of H pattern**, power spectrum cannot capture the nonlinearity, thus we used time domain for estimation.

For the propagation from the *d*H pattern to the non-*d*H pattern, the former was set as the input, and the latter as the fitting target, and *vice versa*. The fitting performance was evaluated by the optimal fitting percentage (FitPercent) among all possible transfer functions, given as

$$\mathrm{FitPercent} = 100\left(1 - \frac{\|y_{\mathrm{measured}} - y_{\mathrm{model}}\|}{\|y_{\mathrm{measured}} - \overline{y_{\mathrm{measured}}}\|}\right)$$

Where y_{measured} is the target output data, $\overline{y_{\mathrm{measured}}}$ is its mean, and y_{model} is the simulated or predicted response of the model. $\|*\|$ indicates the 2-norm of a vector. FitPercent varies between -Infinity (bad fit) to 100 (perfect fit). If the value is zero, the model performs no better at fitting the target than a straight line representing the mean of the data. A higher FitPercent indicates that the model's predicted output closely matches the actual output, signifying superior fitting performance. Therefore, a

higher FitPercent value suggests greater confidence that propagation from the *d*H pattern to non-*d*H pattern is occurring, as the model effectively predicts the outputs of both non-*d*H and *d*H patterns.

Statistical analysis

SPSS 24.0 software was used for statistical analysis. All continuous variables were first tested using a homogeneity test for variance and a test of normality. According to the results, normal variables were presented as mean ± SD; and non-normal variables were reported as medians with interquartile ranges. Categorical variables were displayed as frequencies. Comparisons between two independent groups were made using Student's t tests or nonparametric Mann-Whitney U tests, and comparisons among three independent groups were analyzed with one-way analyses of variance (ANOVAs) or nonparametric Kruskal-Wallis tests. The two correlation groups using Paired Student's t tests or Wilcoxon Signed-Rank Test. Pearson's chi-square or Fisher's exact tests were used for categorical variables. Multivariate logistic regression was used to control for potential confounding factors when comparing the *d*H pattern resection ratio between the two groups. A *P* (Bonferroni adjusted for multiple testing) value < 0.05 was considered statistically significant.

Author Contributions

Conceptualization: S.W., D.-P.Y. Data collection: L.-L.H., L.-Q.Y., H.-Y.Y. Data analysis: L.-L.H., X.-C.L., K.X., Y.-M.Z. Validation of analysis: Z.Z., H.-J.J. Supervision: Z.-J.W., Y.-C.W., K.-J.H. Funding acquisition: S.W., C.C. Writing-manuscript preparation: L.-L.H., D.-P.Y., J.M.Z. Writing-reviewing and editing: S.W., D.-P.Y., J.-P.Z., M.-P.D., C.Z.

Competing Interest Statement

The authors report no competing interests.

Data availability

The collected EEG data are used for seizure localization and to inform clinical decisions. The de-identified dataset supporting the study findings is available upon request from the corresponding author. For inquiries or to request the source data for the figures, please contact S.W. via e-mail.

Code availability

EEG data analyses were performed using the freely available toolbox Brainstorm in combination with custom Matlab scripts, which are available at: https://github.com/chenx-epi/H-pattern.

Acknowledgements

This work was supported by the National Natural Science Foundation of China (grant numbers: 82171437, 82471469 and 82301636) and the Natural Science Foundation of Zhejiang Province (grant no. LD24H090003 and LY24H090004).

Supplementary material

Supplementary material is available online.

References

513 Abeysuriya, R. G., Rennie, C. J., Robinson, P. A., & Kim, J. W. (2014). Experimental observation of a
514 theoretically predicted nonlinear sleep spindle harmonic in human EEG. *Clin Neurophysiol, 125*(10),
515 2016-2023. doi:10.1016/j.clinph.2014.01.025

516 Andrzejak, R. G., Schindler, K., & Rummel, C. (2012). Nonrandomness, nonlinear dependence, and
517 nonstationarity of electroencephalographic recordings from epilepsy patients. *Phys Rev E Stat Nonlin*
518 *Soft Matter Phys, 86*(4 Pt 2), 046206. doi:10.1103/PhysRevE.86.046206

519 Balatskaya, A., Roehri, N., Lagarde, S., Pizzo, F., Medina, S., Wendling, F., . . . Bartolomei, F. (2020).
520 The "Connectivity Epileptogenicity Index " (cEI), a method for mapping the different seizure onset
521 patterns in StereoElectroEncephalography recorded seizures. *Clin Neurophysiol, 131*(8), 1947-1955.
522 doi:10.1016/j.clinph.2020.05.029

523 Bancaud, J., Angelergues, R., Bernouilli, C., Bonis, A., Bordas-Ferrer, M., Bresson, M., . . . Talairach, J.
524 (1970). Functional stereotaxic exploration (SEEG) of epilepsy. *Electroencephalogr Clin Neurophysiol,*
525 *28*(1), 85-86.

526 Bartolomei, F., Chauvel, P., & Wendling, F. (2008). Epileptogenicity of brain structures in human
527 temporal lobe epilepsy: a quantified study from intracerebral EEG. *Brain, 131*(Pt 7), 1818-1830.
528 doi:10.1093/brain/awn111

529 Buzsa´ki, G. (2006). Rhythms of the brain. *New York: OUP*.

Coelli, S., Tacchino, G., Visani, E., Panzica, F., Franceschetti, S., & Bianchi, A. M. (2019). Higher order spectral analysis of scalp EEG activity reveals non-linear behavior during rhythmic visual stimulation. *J Neural Eng*, *16*(5), 056028. doi:10.1088/1741-2552/ab296e

Cole, S., & Voytek, B. (2019). Cycle-by-cycle analysis of neural oscillations. *J Neurophysiol*, *122*(2), 849-861. doi:10.1152/jn.00273.2019

Cole, S. R., & Voytek, B. (2017). Brain Oscillations and the Importance of Waveform Shape. *Trends Cogn Sci*, *21*(2), 137-149. doi:10.1016/j.tics.2016.12.008

David, O., Blauwblomme, T., Job, A. S., Chabardès, S., Hoffmann, D., Minotti, L., & Kahane, P. (2011). Imaging the seizure onset zone with stereo-electroencephalography. *Brain*, *134*(Pt 10), 2898-2911. doi:10.1093/brain/awr238

de Curtis, M., & Gnatkovsky, V. (2009). Reevaluating the mechanisms of focal ictogenesis: The role of low-voltage fast activity. *Epilepsia*, *50*(12), 2514-2525. doi:10.1111/j.1528-1167.2009.02249.x

Devinsky, O., Vezzani, A., O'Brien, T. J., Jette, N., Scheffer, I. E., de Curtis, M., & Perucca, P. (2018). Epilepsy. *Nat Rev Dis Primers*, *4*, 18024. doi:10.1038/nrdp.2018.24

Di Giacomo, R., Burini, A., Chiarello, D., Pelliccia, V., Deleo, F., Garbelli, R., . . . Gnatkovsky, V. (2024). Ictal fast activity chirps as markers of the epileptogenic zone. *Epilepsia*, *65*(6), e97-e103. doi:10.1111/epi.17995

Elgar S, G. R. (1985). Observations of bispectra of shoaling surface gravity waves. *Journal of Fluid Mechanics, 161:425– 448*.

549 Elgar S, S. G. (1989). Statistics of bicoherence and biphase. *J Geophys Res Oceans, 94:10993–10998*.

550 Frauscher, B. (2020). Localizing the epileptogenic zone. *Curr Opin Neurol*, *33*(2), 198-206.

551 doi:10.1097/wco.0000000000000790

552 Fujiwara-Tsukamoto, Y., Isomura, Y., Imanishi, M., Ninomiya, T., Tsukada, M., Yanagawa, Y., . . .

553 Takada, M. (2010). Prototypic seizure activity driven by mature hippocampal fast-spiking interneurons.

554 *J Neurosci*, *30*(41), 13679-13689. doi:10.1523/jneurosci.1523-10.2010

555 Garcia-Rosales, F., Schaworonkow, N., & Hechavarria, J. C. (2024). Oscillatory Waveform Shape and

556 Temporal Spike Correlations Differ across Bat Frontal and Auditory Cortex. *J Neurosci*, *44*(10).

557 doi:10.1523/JNEUROSCI.1236-23.2023

558 Gnatkovsky, V., de Curtis, M., Pastori, C., Cardinale, F., Lo Russo, G., Mai, R., . . . Francione, S. (2014).

559 Biomarkers of epileptogenic zone defined by quantified stereo-EEG analysis. *Epilepsia*, *55*(2), 296-305.

560 doi:10.1111/epi.12507

561 Gnatkovsky, V., Francione, S., Cardinale, F., Mai, R., Tassi, L., Lo Russo, G., & de Curtis, M. (2011).

562 Identification of reproducible ictal patterns based on quantified frequency analysis of intracranial EEG

563 signals. *Epilepsia*, *52*(3), 477-488. doi:10.1111/j.1528-1167.2010.02931.x

564 Gnatkovsky, V., Librizzi, L., Trombin, F., & de Curtis, M. (2008). Fast activity at seizure onset is

565 mediated by inhibitory circuits in the entorhinal cortex in vitro. *Ann Neurol*, *64*(6), 674-686.

566 doi:10.1002/ana.21519

Grinenko, O., Li, J., Mosher, J. C., Wang, I. Z., Bulacio, J. C., Gonzalez-Martinez, J., . . . Chauvel, P. (2018). A fingerprint of the epileptogenic zone in human epilepsies. *Brain, 141*(1), 117-131. doi:10.1093/brain/awx306

He, C., Chen, C., Yang, Y., Hu, L., Jin, B., Ming, W., . . . Wang, S. (2022). Clinical Characteristics and Prognostic Significance of Subclinical Seizures in Focal Epilepsy: A Retrospective Study. *Neurol Ther, 11*(2), 763-779. doi:10.1007/s40120-022-00342-y

Hu, L., Xiong, K., Ye, L., Yang, Y., Chen, C., Wang, S., . . . Wang, S. (2023). Ictal EEG desynchronization during low-voltage fast activity for prediction of surgical outcomes in focal epilepsy. *J Neurosurg, 139*(1), 238-247. doi:10.3171/2022.11.JNS221469

Jehi, L. (2018). The Epileptogenic Zone: Concept and Definition. *Epilepsy Curr, 18*(1), 12-16. doi:10.5698/1535-7597.18.1.12

Jin, B., So, N. K., & Wang, S. (2016). Advances of Intracranial Electroencephalography in Localizing the Epileptogenic Zone. *Neurosci Bull, 32*(5), 493-500. doi:10.1007/s12264-016-0035-8

Jouny, C. C., Adamolekun, B., Franaszczuk, P. J., & Bergey, G. K. (2007). Intrinsic ictal dynamics at the seizure focus: effects of secondary generalization revealed by complexity measures. *Epilepsia, 48*(2), 297-304. doi:10.1111/j.1528-1167.2006.00963.x

Köhling, R., Vreugdenhil, M., Bracci, E., & Jefferys, J. G. (2000). Ictal epileptiform activity is facilitated by hippocampal GABAA receptor-mediated oscillations. *J Neurosci, 20*(18), 6820-6829. doi:10.1523/jneurosci.20-18-06820.2000

Lagarde, S., Buzori, S., Trebuchon, A., Carron, R., Scavarda, D., Milh, M., . . . Bartolomei, F. (2019). The repertoire of seizure onset patterns in human focal epilepsies: Determinants and prognostic values. *Epilepsia*, *60*(1), 85-95. doi:10.1111/epi.14604

Lasztóczi, B., Nyitrai, G., Héja, L., & Kardos, J. (2009). Synchronization of GABAergic inputs to CA3 pyramidal cells precedes seizure-like event onset in juvenile rat hippocampal slices. *J Neurophysiol*, *102*(4), 2538-2553. doi:10.1152/jn.91318.2008

Lévesque, M., Herrington, R., Hamidi, S., & Avoli, M. (2016). Interneurons spark seizure-like activity in the entorhinal cortex. *Neurobiol Dis*, *87*, 91-101. doi:10.1016/j.nbd.2015.12.011

Lévesque, M., Salami, P., Gotman, J., & Avoli, M. (2012). Two seizure-onset types reveal specific patterns of high-frequency oscillations in a model of temporal lobe epilepsy. *J Neurosci*, *32*(38), 13264-13272. doi:10.1523/jneurosci.5086-11.2012

Li, J., Grinenko, O., Mosher, J. C., Gonzalez-Martinez, J., Leahy, R. M., & Chauvel, P. (2020). Learning to define an electrical biomarker of the epileptogenic zone. *Hum Brain Mapp*, *41*(2), 429-441. doi:10.1002/hbm.24813

Marceglia, S., Foffani, G., Bianchi, A. M., Baselli, G., Tamma, F., Egidi, M., & Priori, A. (2006). Dopamine-dependent non-linear correlation between subthalamic rhythms in Parkinson's disease. *J Physiol*, *571*(Pt 3), 579-591. doi:10.1113/jphysiol.2005.100271

603 Müller-Putz, G. R., Scherer, R., Brauneis, C., & Pfurtscheller, G. (2005). Steady-state visual evoked
604 potential (SSVEP)-based communication: impact of harmonic frequency components. *J Neural Eng*,
605 *2*(4), 123-130. doi:10.1088/1741-2560/2/4/008

606 Rosenblatt, M., Van Ness, JW. (1965). Estimation of the bispectrum. *Annals of Mathematical Statistics,*
607 *36:1120 –1136*. doi:10.1007/978-l-4419-8339-8_23

608 Samarasinghe, R. A., Miranda, O. A., Buth, J. E., Mitchell, S., Ferando, I., Watanabe, M., . . . Novitch,
609 B. G. (2021). Identification of neural oscillations and epileptiform changes in human brain organoids.
610 *Nat Neurosci*, *24*(10), 1488-1500. doi:10.1038/s41593-021-00906-5

611 Schiff, S. J., Colella, D., Jacyna, G. M., Hughes, E., Creekmore, J. W., Marshall, A., . . . Weinstein, S. R.
612 (2000). Brain chirps: spectrographic signatures of epileptic seizures. *Clin Neurophysiol*, *111*(6), 953-958.
613 doi:10.1016/s1388-2457(00)00259-5

614 Sheremet, A., Burke, S. N., & Maurer, A. P. (2016). Movement Enhances the Nonlinearity of
615 Hippocampal Theta. *J Neurosci*, *36*(15), 4218-4230. doi:10.1523/JNEUROSCI.3564-15.2016

616 Singh, S., Sandy, S., & Wiebe, S. (2015). Ictal onset on intracranial EEG: Do we know it when we see it?
617 State of the evidence. *Epilepsia*, *56*(10), 1629-1638. doi:10.1111/epi.13120

618 Sivaraju, A., Hirsch, L., Gaspard, N., Farooque, P., Gerrard, J., Xu, Y., . . . Spencer, D. D. (2022).
619 Factors Predicting Outcome After Intracranial EEG Evaluation in Patients With Medically Refractory
620 Epilepsy. *Neurology*, *99*(1), e1-e10. doi:10.1212/WNL.0000000000200569

621 Slaght, S. J., Paz, T., Chavez, M., Deniau, J. M., Mahon, S., & Charpier, S. (2004). On the activity of
622 the corticostriatal networks during spike-and-wave discharges in a genetic model of absence epilepsy. *J*
623 *Neurosci*, *24*(30), 6816-6825.

624 Stam, C. J. (2005). Nonlinear dynamical analysis of EEG and MEG: review of an emerging field. *Clin*
625 *Neurophysiol*, *116*(10), 2266-2301. doi:10.1016/j.clinph.2005.06.011

626 Velazquez, J. L., & Carlen, P. L. (1999). Synchronization of GABAergic interneuronal networks during
627 seizure-like activity in the rat horizontal hippocampal slice. *Eur J Neurosci*, *11*(11), 4110-4118.
628 doi:10.1046/j.1460-9568.1999.00837.x

629 Wang, M. Y., Wang, J., Zhou, J., Guan, Y. G., Zhai, F., Liu, C. Q., . . . Luan, G. M. (2017). Identification
630 of the epileptogenic zone of temporal lobe epilepsy from stereo-electroencephalography signals: A
631 phase transfer entropy and graph theory approach. *Neuroimage Clin*, *16*, 184-195.
632 doi:10.1016/j.nicl.2017.07.022

633 Wang, S., So, N. K., Jin, B., Wang, I. Z., Bulacio, J. C., Enatsu, R., . . . Najm, I. M. (2017). Interictal
634 ripples nested in epileptiform discharge help to identify the epileptogenic zone in neocortical epilepsy.
635 *Clin Neurophysiol*, *128*(6), 945-951. doi:10.1016/j.clinph.2017.03.033

636 Weiss, S. A., Banks, G. P., McKhann, G. M., Jr., Goodman, R. R., Emerson, R. G., Trevelyan, A. J., &
637 Schevon, C. A. (2013). Ictal high frequency oscillations distinguish two types of seizure territories in
638 humans. *Brain*, *136*(Pt 12), 3796-3808. doi:10.1093/brain/awt276

639 Wetjen, N. M., Marsh, W. R., Meyer, F. B., Cascino, G. D., So, E., Britton, J. W., . . . Worrell, G. A.

640 (2009). Intracranial electroencephalography seizure onset patterns and surgical outcomes in nonlesional

641 extratemporal epilepsy. *J Neurosurg, 110*(6), 1147-1152. doi:10.3171/2008.8.Jns17643

642 Wilke, C., Worrell, G., & He, B. (2011). Graph analysis of epileptogenic networks in human partial

643 epilepsy. *Epilepsia, 52*(1), 84-93. doi:10.1111/j.1528-1167.2010.02785.x

644 Ziburkus, J., Cressman, J. R., Barreto, E., & Schiff, S. J. (2006). Interneuron and pyramidal cell

645 interplay during in vitro seizure-like events. *J Neurophysiol, 95*(6), 3948-3954.

646 doi:10.1152/jn.01378.2005

647

648

Figures and Tables

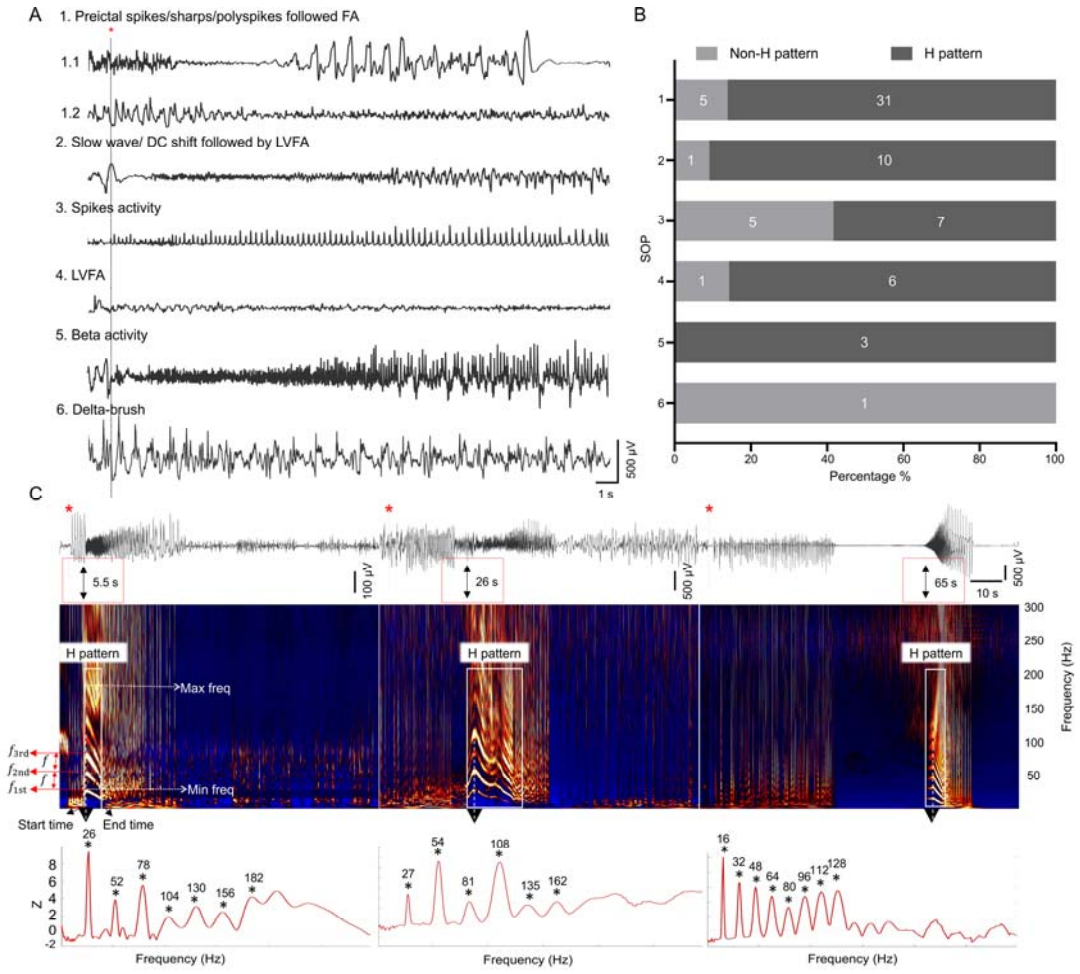

Figure 1 H patterns recorded in seizures with various ictal EEG onset patterns. (A) The six ictal onset patterns defined on iEEG. **(B)** The percentage of patients presenting with certain EEG onset patterns that did or did not exhibit the H pattern. **(C)** EEG (top) and corresponding TFM (middle) during seizures. The TFM shows the 'harmonic pattern (H pattern)': multiple equidistant high-density, narrow bands with varying frequency over time. The initial H patterns presented at various seizure stages on TFM. The black double arrows in the red box mark the start time point of the H pattern. The power

657 spectral density corresponding to the maximal frequency of the H pattern (the black arrow)
658 demonstrates an equidistant distribution of the frequency bands (bottom). The frequency intervals were
659 26, 27, and 16 Hz, respectively. TFM: time frequency map; Max freq: maximal frequency; Min freq:
660 minimal frequency; f_{1st}: the first frequency band, f_{2st}: the second frequency band, f_{3st}: the third frequency
661 band; *f*: fundamental frequency (frequency interval). Red star: seizure onset.
662

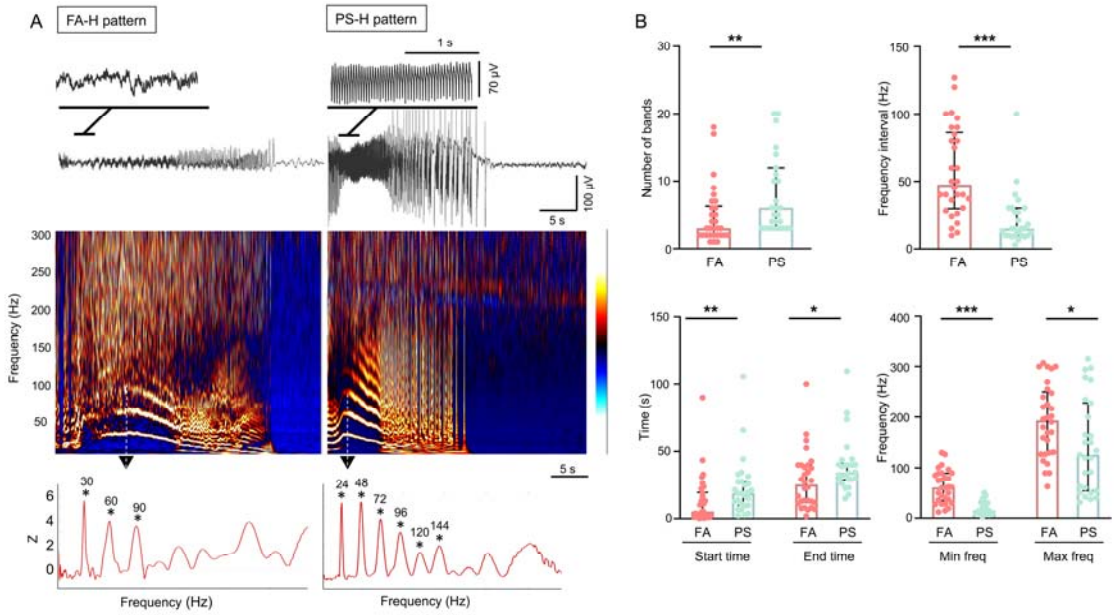

663

664 **Figure 2 Two types of EEG segments harboring H pattern. (A)** H pattern is presented in fast activity
665 (FA-H pattern) and irregular polyspikes (PS-H pattern) (top and middle). The power spectral density
666 (bottom) at the maximal frequency point shows an equidistant distribution of the frequency bands. **(B)**
667 Comparison of parameters between the FA-H pattern and PS-H pattern. The former showed a fewer
668 number of frequency bands (3 (4) vs. 6 (8)), higher frequency interval (47.5 (56.75) vs. 15 (20.00) Hz),
669 earlier start (5.2 (18.19) vs. 18.70 (17.20) s) and end (25.4 (28.30) vs. 33.9 (11.70) s) time, and higher

670 minimal (60 (54.70) vs. 15.00(20.00) Hz) and maximal (193.00 (120.75) vs. 126.00 (159.00) Hz)
671 frequencies than the latter. *P < 0.05; **P < 0.01; ***P < 0.001. Max freq: maximal frequency; Min freq:
672 minimal frequency.

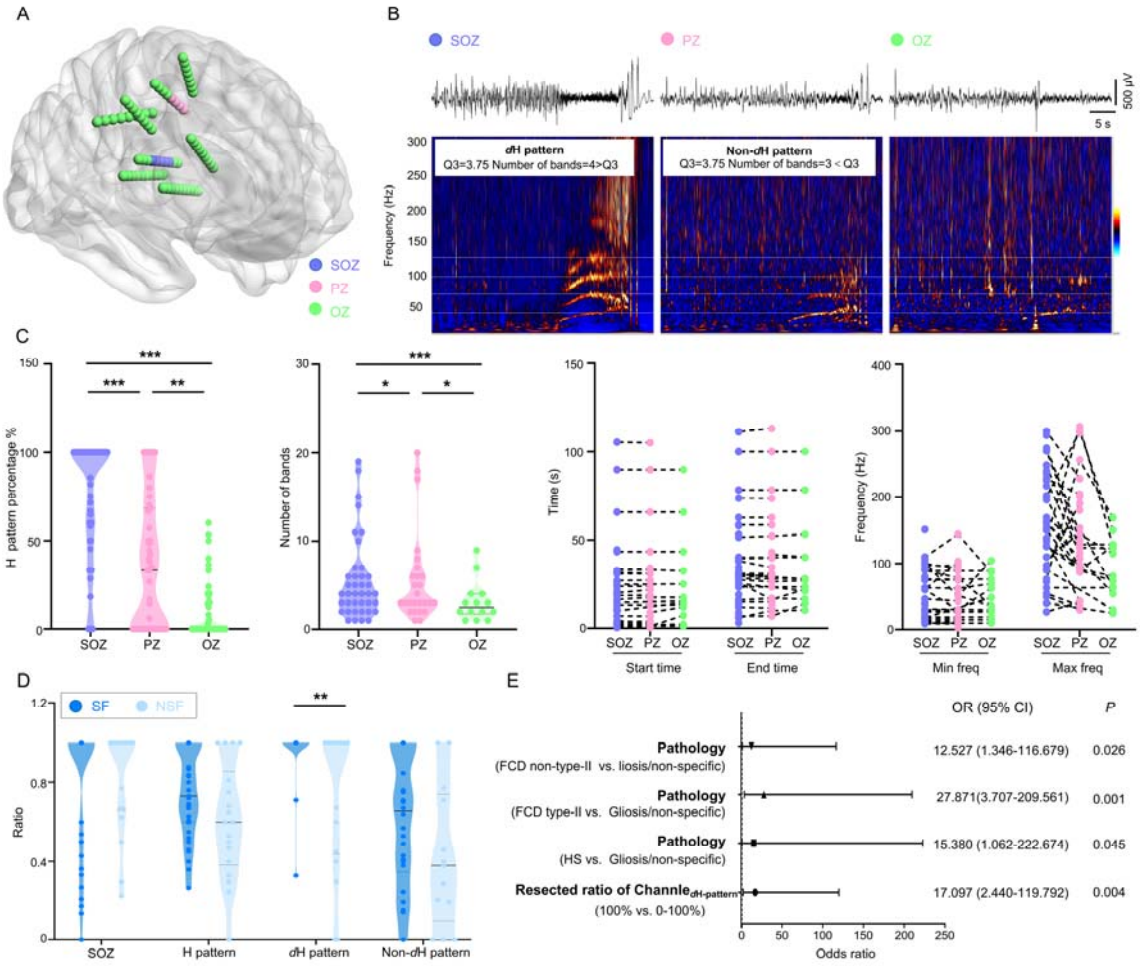

673

674 **Figure 3 Distribution of the H pattern. (A)** Anatomical distribution of SOZ, PZ, and OZ in a patient
675 (left panel). In this case, SOZ is located in the precentral gyrus with early propagation to the postcentral
676 gyrus. The right panel **(B)** shows the corresponding EEG recordings from SOZ, PZ, and OZ, along with
677 the observed H pattern. Red stars indicate seizure onset. **(C)** Comparison of parameters among SOZ,

678 PZ, and OZ in group data. The distribution percentage and the number of bands of H pattern decreases
679 in the order of SOZ, PZ, and OZ (Percentage%: SOZ: 100 (40), PZ: 33 (68), OZ: 0 (13). Number of
680 bands: SOZ: 4 (4), PZ: 2 (4), OZ: 0 (2)). **(D)** Resection of SOZ, H pattern, the *d*H pattern or non-*d*H
681 pattern and surgical outcome. **(E)** Multivariate logistic regression analysis. *$P < 0.05$; **$P < 0.01$; ***$P <$
682 0.001. Max freq: maximal frequency; Min freq: minimal frequency; SOZ: seizure onset zone; PZ: early
683 propagation zone; OZ: other zone. *d*H pattern: dominant H pattern.

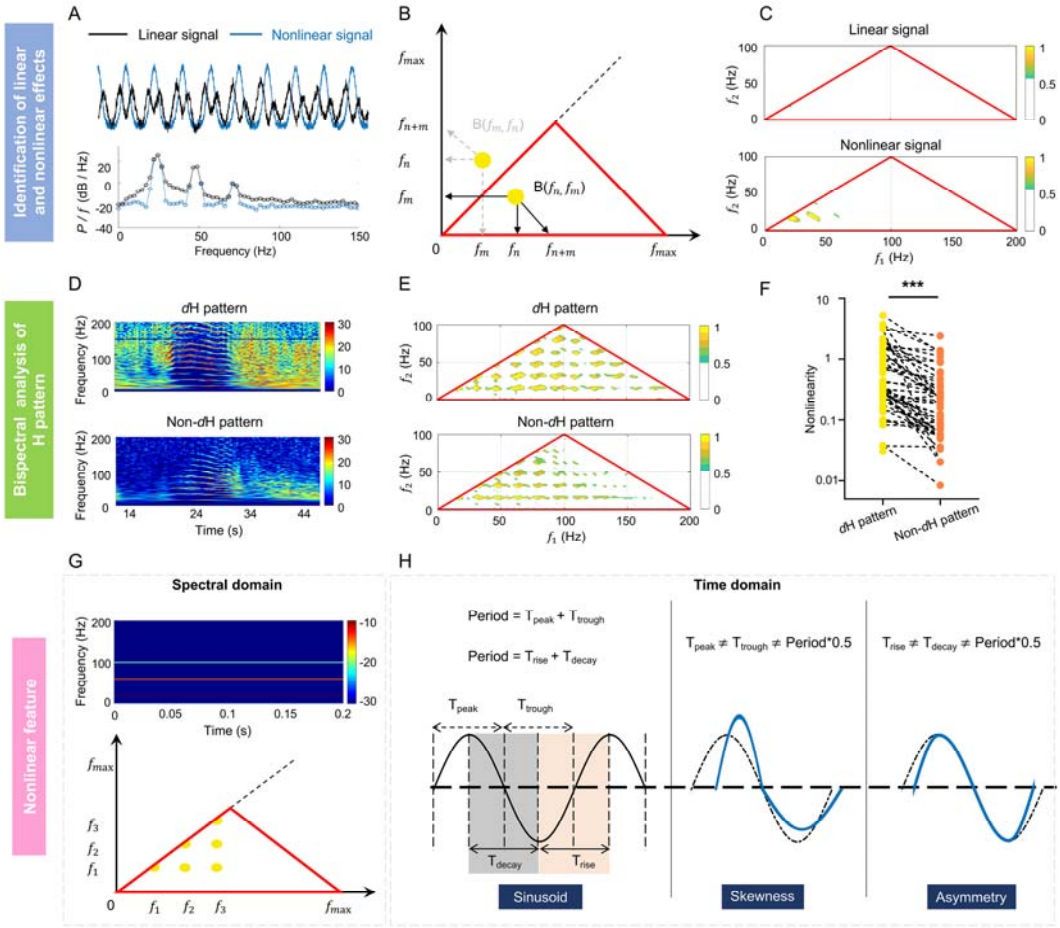

684

685 **Figure 4 Nonlinear analysis of H pattern.**

Identification of linear and nonlinear effects: **(A)** Linear and nonlinear signals (top) and their PSD (bottom). PSD analysis cannot distinguish between linear and nonlinear time series, as these two oscillations have similar spectral density characteristics. **(B)** Bispectral symmetry. The first diagonal serves as the axis of symmetry, with data on both sides being identical, and the red triangle represents the area containing nonredundant bispectral information. The peak in the bispectral estimate (yellow dot) represents a phase-coupled triplet (f_n, f_m, f_{n+m}). If a bispectral peak (yellow dot) is on the first diagonal, then $m = n$, meaning that frequency f_n is phase correlated to its second harmonic $f_{2n} = 2f_n$. **(C)** Normalized bispectrum of linear and nonlinear signals. Bispectral analysis can distinguish the linear and nonlinear characteristics of signals: the normalized bispectrum and all of its components for linear signal are approximately zero, whereas nonlinear signal exhibits four prominent peaks.

Bispectral analysis of H patterns: **(D)** Example of the *d*H and non-*d*H patterns. **(E)** Example of normalized bispectrum for the *d*H and non-*d*H patterns. In comparison to the non-*d*H pattern, the *d*H pattern exhibits more bicoherence peaks, signifying the presence of stronger harmonic phase coupling. **(F)** Comparison of bispectral values between the *d*H patterns and non-*d*H patterns in group data.

Features of nonlinear effects: **(G)** In the spectral domain, nonlinearity is expressed as a series of harmonics that are phase-locked to the fundamental frequency, as evident in both TFM (top) and bispectral analysis (bottom). **(H)** In the time domain, nonlinearity is manifested as the asymmetry and skewness of the waveform. The left side uses a sinusoidal wave example to illustrate the period, peak, trough, rise, and decay. The distorted blue waveforms on the right, relative to the sinusoidal wave

706 (black dashed line), exemplify skewness and asymmetry. PSD: power spectral density; DFT: discrete

707 Fourier transform; TFM: time frequency map.

708

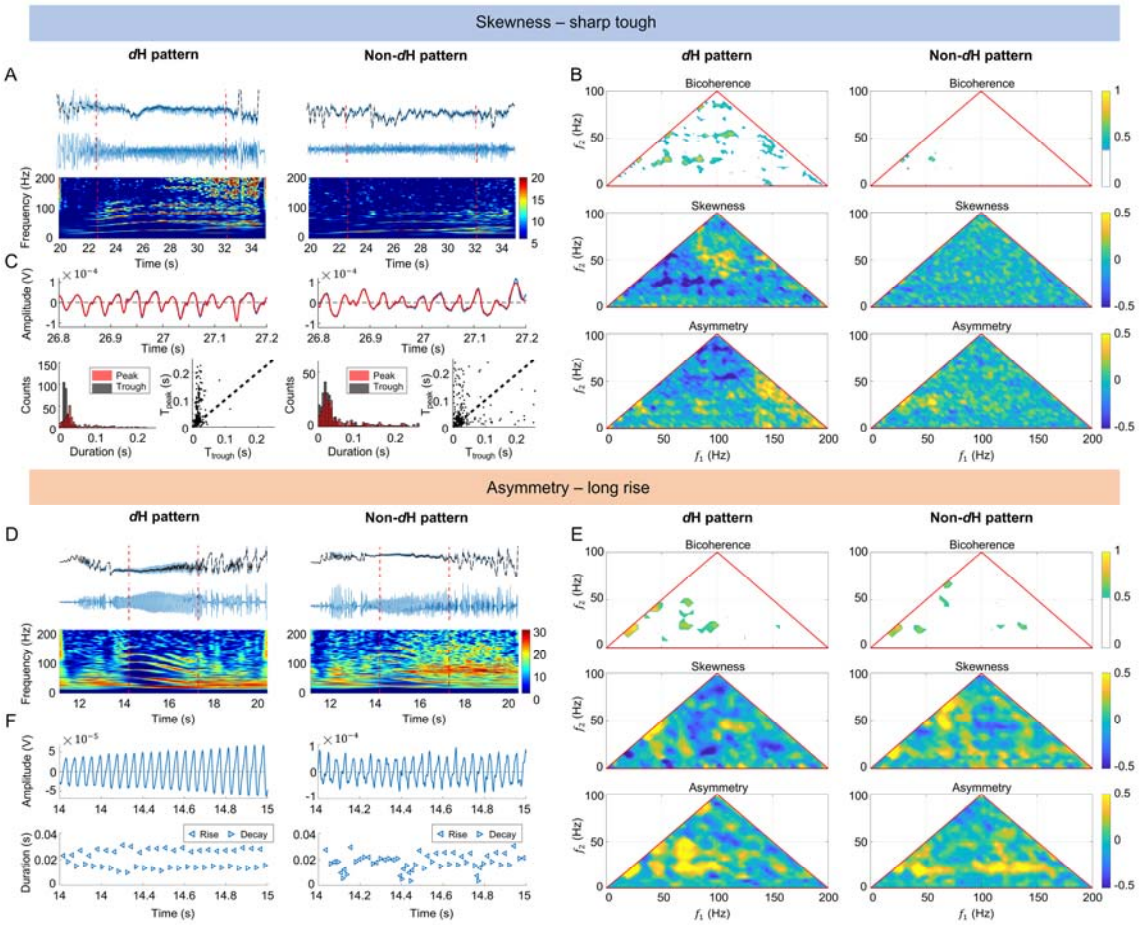

709

710 **Figure 5 Waveform analysis of H pattern.** ***The dH pattern is attributed to stronger skewness***

711 ***(sharper trough).*** **(A)** Original iEEG signals in the *d*H/non-*d*H patterns (top), detrended iEEG signals

712 (middle), TFM (bottom); **(B)** Bispectral analysis for the *d*H/non-*d*H patterns. **(C)** Comparison of peak

713 and tough. Top: peaks and troughs (blue lines) in the *d*H/non-*d*H patterns are separately fitted by sin

714 waves (red lines), respectively; Bottom: Histogram (left) and scatter plot (right) depicting the distribution

715 of T_{peak} vs. T_{trough} for the *d*H/non-*d*H patterns.

The dH pattern is attributed to stronger asymmetry (longer rise). **(D)** Original iEEG signals in the *d*H/non-*d*H patterns (top), detrended iEEG signals (middle), TFM (bottom). **(E)** Bispectral analysis for the *d*H/non-*d*H patterns. **(F)** Comparison of rise and decay. Enlarged plots of detrended iEEG signals (top) and the corresponding rise (left triangles) and decay (right triangles) (bottom). The black dashed line in **A and D** represents the smoothed signals. The time with H pattern is marked by the red dotted vertical lines.

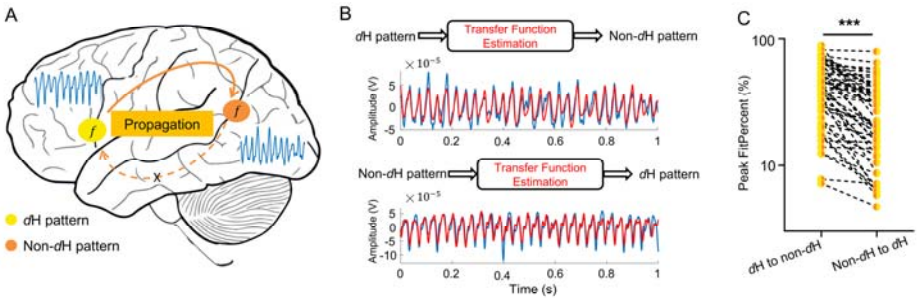

Figure 6 Propagation analysis of H pattern (A) Schematic of signal propagation from region with the *d*H pattern to one with the non-*d*H pattern but not the opposite. The two regions share the same fundamental frequency (*f*). **(B)** Top: Estimating a transfer function with the input of *d*H pattern to fit non-*d*H pattern. Bottom: Estimating a transfer function with the input of non-*d*H pattern to fit *d*H pattern (blue: the input signal, red: the fitting signal). **(C)** Comparison of peak FitPercent between propagation from the *d*H pattern to the non-*d*H pattern and its opposite. **P* < 0.05; ***P* < 0.01; ****P* < 0.001. *f*: fundamental frequency.

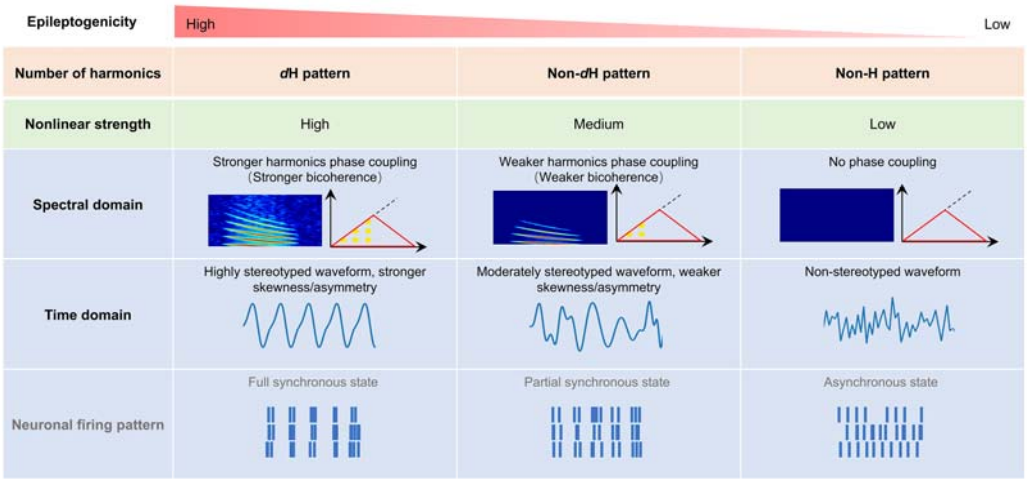

732

733 **Figure 7 Summary of the nonlinear features for H pattern.** The epileptogenicity, as reflected by the
734 nonlinear features of H pattern, exhibits a clear gradient of decrease from the *d*H pattern to non-*d*H
735 pattern, and is notably diminished in the non-H pattern. In the spectral domain, this is seen as a decline
736 in harmonic numbers in TFM and coupled peaks in bispectral analysis. In the time domain, the decline
737 is marked by reduced skewness and/or asymmetry of waveforms, with the *d*H pattern correlated with
738 more stereotyped waveforms. It is hypothesized that the harmonic nonlinearity reflects the
739 synchronization level of neuronal firing, which decreases from the *d*H pattern to non-*d*H pattern and is
740 absent in the non-H pattern.

741

742 **Table 1** Clinical characteristics and surgical outcomes in patients with focal onset pattern on iEEG.

	Total (n = 57)	Seizure-free (Engel class Ia) (n = 39)	Not-seizure free (> Engel class Ia) (n = 18)	*P* value
Gender, M, n (%)	31 (54.4 %)	20 (51.3 %)	11 (61.1 %)	0.489[b]
Age at onset, y	10.4±8.5	9.4±7.5	12.6±10.2	0.193[a]
Age at surgery, y	23.6±12.3	23.6±12.8	23.7±11.3	0.991[a]
Epilepsy duration, y	13.3±11.2	14.2±11.8	11.1±9.6	0.329[a]
EEG segments with H pattern, FA/PS	30/27	20/19	10/8	0.764[b]
Lateralization, L, n (%)	26 (45.6 %)	18 (46.2 %)	8(44.4 %)	0.904[b]
Epileptogenic lesion on MRI, n (%)	49 (85.9 %)	35 (89.7 %)	14 (77.8 %)	0.246[c]
Localization, n (%)				0.243[c]
Temporal	20 (35.1 %)	10 (25.6 %)	10 (55.6 %)	
Frontal	24 (42.1 %)	18 (46.2 %)	6(33.3 %)	
Parietal	4(7.0 %)	3 (7.7 %)	1(5.6 %)	
Occipital	4(7.0 %)	4(10.3 %)	0(0.0 %)	
Multi-lobar	5(8.8 %)	4(10.3 %)	1(5.6 %)	
Pathology, n (%)				0.004[c]
Hippocampal sclerosis	6(10.5 %)	5 (12.8 %)	1 (5.6 %)	
Focal cortical dysplasia type II	28 (49.1 %)	23 (59 %)	5 (27.8 %)	
Focal cortical dysplasia (non-type II)	11 (19.3 %)	7(17.9 %)[d]	4 (22.2 %)[d]	
Tumor	2 (3.5 %)	2(5.1 %)	0(0.0 %)	
gliosis/non-specific	10 (17.5%)	2 (5.1 %)[e]	8 (44.4 %)[e]	

743 Abbreviations: iEEG: intracranial electroencephalography. M: male; y: years; H pattern: harmonic
744 pattern; FA: fast activity; PS: periodic spike; L: left; MRI: magnetic resonance imaging; SF: seizure free;
745 NSF: not seizure free. Data are presented as the number of patients for categorized variables and the
746 mean ± standard deviation for continuous variables. a. Unpaired, two-tailed t-tests. b. Pearson's
747 chi-square test. c. Fisher exact test. d & e. Bonferroni correction: In the SF and NSF groups, there was
748 a discrepancy in pathological finding (*P* = 0.004). A significant difference was found between FCD II
749 and gliosis/non-specific findings.